# Expanding plasma used for plasma deposition

Please check the document version of this publication:

• A submitted manuscript is the version of the article upon submission and before peer-review. There can be important differences between the submitted version and the official published version of record. People interested in the research are advised to contact the author for the final version of the publication, or visit the DOI to the publisher's website.
• The final author version and the galley proof are versions of the publication after peer review.
• The final published version features the final layout of the paper including the volume, issue and page numbers.

[Link to publication](Link to publication)

# Expanding plasma used for plasma deposition

G.M.W. Kroesen, C.J. Timmermans and D.C. Schram


Department of Physics, Eindhoven University of Technology
P.O. Box 513, 5600 MB, Eindhoven, The Netherlands

Abstract. A description of the deposition process for the production of
amorphous carbon coatings, based on decomposition of hydrocarbons in a new
type of plasma reactor, is presented. In this reactor the dissociation and
ionization of the original, carbon containing material takes place follo-
wing injection in the thermal high density plasma of a cascaded arc. This
plasma is close to local thermal equilibrium (LTE). The hot seeded arc
plasma is cooled by allowing it to expand supersonically into a large va-
cuum system. In the expansion high particle velocities are attained, ensu-
ring that the plasma composition does not change substantially before the
substrate is reached. At the substrate an amorphous carbon film is deposi-
ted with rates up to 200 nm/s, which are measured with in-situ ellipsome-
try. The quality of this film, determined by parameters like refractive
index, hardness, absorption coefficient in the infrared spectral region,
resistance against oxidation, adhesion to the substrate and internal
stress, is strongly dependent on the plasma parameters. These parameters
can be controlled easily so the intensity and conditions of the particle
flux impinging on the substrate can be influenced. Plasma parameters such
as electron density, temperatures as well as drift velocities have been
measured.

## INTRODUCTION

Amorphous carbon coatings have a number of industrial and scientific applications. Because of
the low absorption coefficient in the infrared region they are frequently used in antireflex
and/or protective coatings for that spectral area. Their (generally) high refractive index
makes them applicable where an index gradient is required like in the case of optical fibers
used for data transportation. Also as protective coatings for solar cells or integrated cir-
cuits they can be interesting, although in most applications of this kind the internal stress
of many kinds of the material inhibits use on thin silicon slices. In tribological applica-
tions this material strongly enhances the surface hardness of treated parts in machines,
turbines and engines.

Since about 1970 many different discharge types have been explored for their applicability in
the field of plasma surface modification in general and of plasma deposition in particular.
By far the most widespread deposition process comprises the use of an RF or DC glow discharge
in a mixture of a noble gas like argon, hydrocarbons and sometimes oxygen (ref. 1), contac-
ting the surface to be treated. Often the sample support is negatively biased to increase the
intensity of the ion bombardment. The hydrocarbons are dissociated in the plasma glow and are
transported towards the substrate by means of diffusion. Among others Matsushita et al (ref.
2), Donahue et al (ref. 3) and Vanier et al (ref. 4) use glow discharges and attain deposi-
tion rates ranging from 0.3 to 3 nm/s which are in this case mainly limited by the effecti-
vity of the transportation of the particles towards the area where the coating is formed, but
also by the effectivity of the production of these reactive particles. This proces is usually
called "plasma deposition".
Wong et al (ref. 5) makes use of a nozzle beam, whereas Ebihara et al (ref. 6) and Sokolowski
et al (ref. 7) have investigated a pulsed discharge. In industrial processes ion plating has
gained much interest recently, see e.g. Umeda et al (ref. 8), especially for coatings that
require a large energy flux impinging on the surface. Of course evaporation (thermal or elec-
tron induced) has to be mentioned. This technique is applied in a number of commercially
available reactors. Shindo et al (ref. 9) reported good results with a modified evaporation
process using a reactive gas. Afterglows of inert gases can also be used to dissociate and
sometimes ionize (fragments of) the reactive gas, see e.g. Toyoshima et al and Watanabe et al
(refs. 10, 11). Usually the metastable atoms play an important role in the reaction kinetics.
Hollow cathode glow discharges are used to sputter material from a solid reactant, e.g.
Matsumura et al (ref. 12). A more energetic version of this discharge type, a hollow cathode

arc, is used for the same purpose by Lunk et al (ref. 13). Zarowin et al (ref. 14) has developed a method based on chemical vapour transport of particles evaporated from solid material. Even multipole discharges are used for the production of coatings of various materials (refs. 15, 16). The industry often uses microwaves to dissociate the gas (ref. 17).
Another technique, called "Ion Beam Epitaxy" (IBE) uses a beam of ions accelerated on its way to the substrate (e.g. ref. 18). The deposition rates obtainable with this technique are strongly dependent on the reactor geometry, but usually also values about 0.3-3 nm/sec are obtained. In this case the limit is primarily set by the production of the reactive particles (ions).

As can be learned from these techniques, the plasma conditions (pressure, power density, gas flow, composition of gas mixture, electrode geometry, etc.) play a dominant role in the deposition process: on one hand they determine the decomposition of the gas and on the other hand they determine the surface conditions which are important for the layer quality. It is not certain that in conventional plasma deposition devices these two demands can be totally met for one set of plasma conditions. Generally a situation which favours a fast dissociation of the gas has a negative influence on the surface conditions. If the location where the gas will be dissociated is spatially separated from the surface where the deposition takes place both processes are individual controllable. Furthermore, a higher deposition rate can be attained if the reactive particles are transported to the surface in an active way rather than by diffusion.

So, if the transport properties of an ion beam can be combined with the dissociative and ionizing power of a dense discharge without losing much of the plasma volume by collimation we will fulfil the foregoing requirements. Then the process control and more specifically the deposition rate can be increased substantially. This combination is realized in this study by the injection of a carbon containing material into a thermal (gas temperature equals electron temperature) high density plasma of a wall-stabilized cascade arc and by allowing this hot seeded dense plasma to expand freely through a hole in the anode of this cascade arc into a large vacuum vessel. Then an intense plasma beam is formed, with a large systematic velocity and an increasing effective area. In this way the plasma production is geometrically separated from the plasma treatment which gives more freedom to optimize the process.

If necessary the energy of the (electrically charged) particles impinging on the substrate to be treated can be further increased by creating an auxiliary discharge (DC or RF) at the location of the (in this case water cooled) sample support.

In this study we will discusse the model on which development of this new type op deposition reactor is based, the reactor itself and the various diagnostics which are used to determine the plasma parameters.

As an example some results of the deposition of amorphous hydrogenated carbon coatings from a mixture of methane, acetylene, hydrogen and argon will be discussed. Deposition rates up to 200 nm/s will be reported. The resulting films are often called 'diamond-like' since their physical parameters like hardness, refractive index and absorption coefficient show a strong similarity to the diamond values.

The electron density, the electron temperature and the gas pressure inside the cascade arc channel have been determined as a function of axial position for a number of discharge conditions and the results will be discussed.
The expanding plasma beam can be observed with an optical system comprising a 0.5 m monochromator and a Fabry-Pérot interferometer. The electron density is determined using the Stark broadening of the Hβ-Balmer line (486.1 nm). The gas velocity can be deduced from the Doppler shift of the 420.0 nm argon neutral line, the gas temperature from the width of the Gaussian component of the same line.
The deposition rate is measured using in-situ He-Ne ellipsometry at a wavelength of 632.8 nm. This technique also yields the refractive index and the absorption coefficient of the produced film at this wavelength. The optical properties over a wide wavelength area have been determined using spectroscopic ellipsometry.

## POSSIBILITIES AND LIMITATIONS OF PLASMA DEPOSITION PROCESSES

Although the given variety of devices is far from complete, it may be clear that a plasma can be used in a number of ways to enhance the performance of the deposition processes when compared to chemical vapour deposition (CVD). We will discuss some physical aspects of the plasma deposition process on the basis of a model in which the plasma – surface system is subdivided into three stages, viz.
1. dissociation and partial ionization of the molecules of the gas to be used in the process (the plasma production phase),
2. transportation of the fragments towards the surface to be treated and
3. (chemical) reaction of the fragments on the surface.
In each of these stages the plasma properties may play a decisive role. In the usual approach these stages take place in the same volume. In the studied reactor however, the plasma pro-

duction (the dense cascaded arc plasma) is geometrically separated from the transportation of the radicals and ions to the surface (the seeded expanding plasma beam). With this separation the production of charged particles will be independently controllable and is removed from the surface to be treated. In this paper we will not dwell on the complicated plasma dynamics; we only quote the observed limitations in radial expansion of the plasma beam due to the slow ambipolar diffusion compared to the plasma drift velocity. We only want to discuss, in general terms, the balance of production and loss in the three regions of the proposed model; the role of the photons will be ignored.

The three phase model is depicted in Fig. 1 and for each of the three volumes the mass conservation law is valid:

$$\iiint_V \left.\frac{\partial n}{\partial t}\right|_{Prod} dV = \iint_S n\underline{w}\cdot d\underline{S}. \tag{1}$$

Here $(dn/dt)_{Prod}$ means the net production rate (production minus losses) of the reactive particles $n$ involved in the volume $V$; $\underline{w}$ means their drift velocity, so $n\underline{w}$ is the flux passing the surfaces $S$.
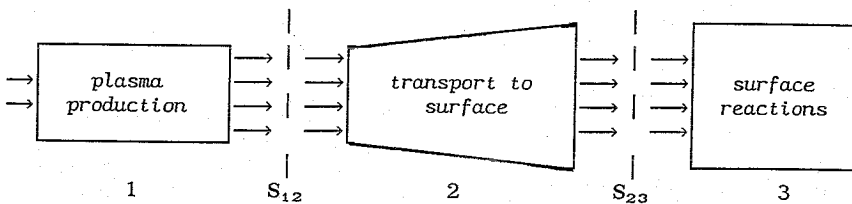


Fig. 1. Model of the three phases of the plasma deposition process.

For an optimum plasma flow emanating from production section -1- to transport section -2- (see Fig. 1), a large net production $(dn/dt)_{Prod}$ and a minimum of radial losses are required. One can approximate the net production term by

$$\left.\frac{\partial n}{\partial t}\right|_{Prod} = n_{fe}\ n_e\ k. \tag{2}$$

In words: the production rate is proportional to the density of the feeding material $n_{fe}$, the electron density $n_e$ (supposing the electrons primary induce the reactions) and the rate constant for excitation, dissociation and ionization $k$. The rate constant depends strongly on the electron temperature.

It is advantageous to increase $n_{fe}$ and $n_e$. The ionization degree (rate electron density to gas density) of a atmospheric thermal plasma is in the order of 10 % for argon (ref. 19, 20). Since there will be a preference for particles of low ionization potential full dissociation and substantial ionization of the seeded material, e.g. $CH_4$, is attained.

The main advantages of the use of a thermal plasma of a cascaded arc as plasma production are: small plasma source dimensions (4 mm diameter, length 60 mm), a very dense plasma (particle densities up to $10^{22}$ $m^{-3}$) and a large total power (up to 10 kW). The latter is relatively high if compared with the normally used glow discharges and hollow cathode arcs. From investigations inside the thermal plasma production section (see also ref. de HAAS), we learned that the plasma composition and temperature hardly change, as will be discussed later. So, with the application of the cascaded arc in this reactor we fulfil the requirements mentioned above for the plasma production region.

To achieve the highest possible flux $n\underline{w}$ from the 'plasma production' region -1- to the 'transportation' region -2- the seeded plasma is allowed to expand freely into a large vacuum system through a hole (4 mm diameter) in the anode of the cascaded arc with a large systematic drift velocity $\underline{w}$ of over $10^3$ m/s.

In the second section -2- (transportation) there are two relevant parameters: the ratio $R$ of the incoming flux of reactive particles trough $S_{12}$ to the flux impinging on the surface $S_{23}$ to be treated, written as

$$R = \iint_{S_{12}} n\underline{w}\ d\underline{S} \Big/ \iint_{S_{23}} n\underline{w}\ d\underline{S} \tag{3}$$

and the loss $(\partial n/\partial t)_{Rec}$ of reactive particles during transport. Again $(\partial n/\partial t)_{Rec}$ depends on the relevant temperatures and on the densities of the involved particles. The requirements in the transportation section are that $R$ approaches unity which implicitely includes a minimum of $(\partial n/\partial t)_{Rec}$. The analogon of eq. (2) learns that the loss is proportional to the relevant densities and also depends on the temperatures. In the supersonic expansion the plasma is accellerated in the forward direction. The supersonic expansion is limited by a shock wave

(barrel shock and Mach disk) which occurs on the place where the mean momentum of the particles inside the expansion equals the mean momentum of the background gas. After the shock wave the velocity of the seeded plasma flow decreases from about 2500 m/s to about 1000 m/s; still a highly directed intensely radiating plasma beam is observed. In the 'transportation' region the plasma expands slowly radially due to the ambipolar diffusion. Carbon atoms which arrive unionized in the transportation section will subsequently be ionized by charge exchange with argon ions. In advance to the results, we will mention here that in the transportation section the temperature drops roughly from 5000 K (from 20 mm after the nozzle) to 3000 K at a distance of 200 mm and to roughly 1500 K at 460 mm. The electron density drops from about $10^{20}$ m$^{-3}$ to $10^{19}$ m$^{-3}$ over the same distance. Due to the high axial velocity the relative composition in the seeded expanding plasma beam will not change considerably and in this way we expect that the rate $R$ between the incoming flux from the nozzle and the outgoing flux to the target will approach unity.

In the third section (surface reactions) the dominant aspects are the ratio $R$ of incoming and outgoing fluxes (in this case strongly related to the sticking probability) and the surface reaction rate $\partial n/\partial t$. The surface reaction rate strongly depends on the potential energy of the reactive particles and on the surface temperature. The surface temperature in its turn is also influenced by the energy of the incoming particles, so the total reaction rate depends strongly on this energy.

From the above considerations one can summarize that the efficiency of a plasma deposition process can be promoted as is indicated in the next list.

         Increasing in
Phase 1: 1. the density of the admixed material,
 ,,      2. the electron density,
 ,,      3. the electron temperature,
 ,,      4. and the gas temperature;
         Also increasing in
Phase 2: 5. the velocity with which the reactive particles emanate from the plasma
            production section and
 ,,      6. the flux ratio $R$;
         And decreasing in
Phase 2: 7. the density of reactive particles and
 ,,      8. the relevant temperatures in order to minimize the volume losses;
         And by in
Phase 3: 9. Increasing the potential energy of the reactive particles impinging
            on the substrate.

In the concluding remarks we will compare the properties of a glow discharge and those of this new type of deposition reactor regarding the afore cited items.


## EXPERIMENTAL DEVICE AND DIAGNOSTICS

### Introduction
As already stated before in the introduction the reactor, which is used in the experiments, combines the transport properties of an ion beam with the dissociative and ionizing power of thermal plasma generated in a cascaded arc. The reactive gas is injected either in the dense arc plasma itself or further downstream in the expansion area. The cascaded arc is of a special design to allow for the injection of methane avoiding both the destruction of the electrodes and the creation of a short-circuit between two adjacent cascaded plates caused y graphite deposition in the arc channel.
Through a hole (4 mm diameter) in the anode the plasma is allowed to expand freely into a large vacuum system where it shows supersonic behaviour. Since the medium expands into vacuum the transport velocity and the effective area in the expanding beam increase. Opposing the arc an electrically floating and water cooled sample support of about 65 mm is mounted. It is possible to create an auxiliary discharge between sample support and vacuum system which influences the intensity of the ion bombardment. Figure 2 presents an outline of the plasma deposition reactor.

As we use a thermal plasma we would like to comment that thermal plasmas in general are increasingly used in technological processes. Atmospheric plasma jets are used in plasma spraying and plasma welding and cutting. A method of ultra fine powder production (UFP) using thermal plasmas for evaporation of metals is called "Plasma Evaporation Process" (ref. 21). High power transferred arcs are employed for melting metal ores in large ovens. Inductively coupled plasmas (ICP's) at moderate power levels are used in spectrochemistry. High power ICP's are applied in gas synthesis reactors. High pressure short arcs in xenon are utilized as a bright light sources.

In this chapter the experimental set-up and the diagnostic techniques will be described. Firstly a view of the plasma generation reactor will be given. Then the vacuum system and the

auxiliary discharge will be briefly discussed. The next section depicts the optical systems as they are used for the various spectroscopic techniques. Finally the practical implementation of ellipsometry and the data acquisition system will be discussed concisely.

## The reactor

The cascaded arc. The cascaded arc was introduced in 1956 by Maecker (ref. 22). Until now it has been applied mainly for investigations of scientific interest. This type of wall stabilized arcs plasmas can be operated under a wide range of pressures (0.1 - 1000 bar) and currents (5 - 2000 amps.), and is characterized by high electron densities ($10^{22} - 10^{23}$ m$^{-3}$), high ionization degrees ($\geq 10$ %) and moderate temperatures (10000 - 16000 K). Mostly noble gases or hydrogen are used to feed the plasma, but exceptionally molecular gases like SF$_6$ are added (e.g. refs. 23, 24]. The deviations from local thermal equilibrium (LTE) have been studied by numerous authors (e.g. refs. 19, 20, 25, 26). At very high electron densities ($10^{24}$ m$^{-3}$) the non-ideal plasma behaviour has been explored (refs. 27, 28). Recently de Haas has investigated the physics of a strongly flowing cascaded arc plasma (ref. 29).

In this study a cascaded arc is employed to dissociate and ionize molecular gases. Therefore a special design has been used (see Fig. 3). Basically the arc consists of an anode, a stack of electrically insulated copper plates and three cathodes, all water cooled. The cathodes are made of thoriated tungsten. The diameter of the tungsten tips is 1 mm for currents up to 30 Amperes per cathode, and 2 mm for higher currents. The thorium which is present in the material segregates to the surface and increases the electron emission. This allows operation at lower temperatures, and prevents the material from melting. The cathode tips are the only parts of the arc system that show any wear. They have to be replaced after about 500 operating hours. The cathode shafts can be removed without taking apart the rest of the construction, so the exchange of the tips only costs a few minutes.
The water cooled cathode support also incorporates a window through which the arc channel can be observed end-on. The gas is fed through the shaft on which this window is mounted.
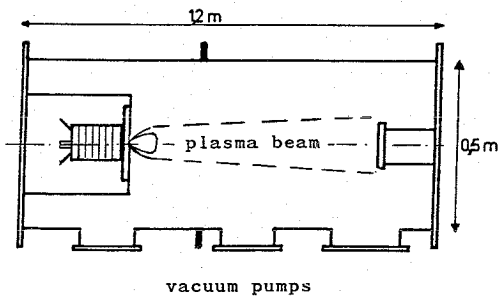


Fig. 2. Outline of the plasma deposition reactor used in the present experiments.
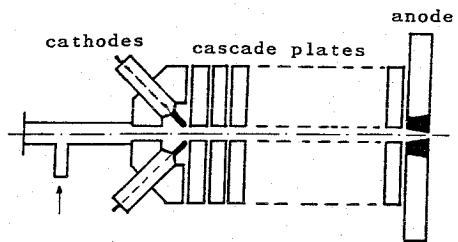
Fig. 3. Schematic view of the cascaded arc.

The cascade plates itself are of a simple design. They consist of a copper plate with a central bore of 4 mm, which is surrounded by a channel through which the cooling water is flowing. The plate thickness is 5 mm. The arc channel is formed by the central bores of the 10 stacked plates which are kept at a vacuum sealed interspacing of 1 mm. When methane is injected into the arc channel special precautions have to be taken to prevent graphite deposition on the walls which would lead to a short-circuit of the plates.
For diagnostical reasons (measurement of the electron density and electron temperature of the arc plasma), special plates has been constructed that allow side-on observation of the plasma through small quartz windows as well as measurement of the pressure in the arc channel as a function of the axial position. The anode nozzle is made of copper.

The complete arc is fixed to the anode supporting flange, which is attached to the vacuum system. As the vacuum system is grounded, the anode is grounded too. Resistors of 4 Ohm in the cathode supply lines make sure that all three cathodes are 'burning' independently.

Vacuum system and gas handling. The vacuum vessel consists of a stainless steel cylinder with a length of 1.2 m, and a diameter of 0.5 m, see Fig. 2. It incorporates several windows and flanges that allow for the execution of various diagnostics. The end flanges are fixed to the cylinder with hinges, and they can be opened and closed easily. On one 'door' the cascaded arc is mounted onto a cylinder that can slide in another cylinder over a length of 0.2 m while the vacuum is maintained. This allows axial motion of the arc in the vacuum system without the need of pressurizing. On the other 'door' the sample support is attached. It can

be moved axially over a distance of about 1 meter while maintaining vacuum (also a sliding O-ring construction), and is electrically insulated from the vacuum system to allow for the creation of an auxiliary discharge.

Essentially two pumping lines are used (see Fig. 2). The first one is used when the reactor is operated. It incorporates a mechanical rotary piston pump and two roots blowers, and is connected to the vacuum vessel by a steppermotor controlled valve. This system makes it possible to set the pumping speed from 10 l/sec up to 700 l/sec. In this way the working pressure in the system and the gas flow can be controlled independently.
The second pumping line consists of a rotary pump and an oil diffusion pump. It is used when the reactor is not operated and keeps the background pressure below $10^{-6}$ mbar.
The gases are fed through mass flow controllers. Argon and hydrogen are supplied at the arc entrance, whereas methane is added in the arc channel.
Table 1 lists the experimental conditions that are used during the measurements described in this work.

Table 1. Experimental conditions

| | | |
|---|---|---|
| arc current | | 20-70 A |
| arc voltage | | 50-150 V |
| arc pressure | | 0.1-5 bar |
| gas flow | argon | 0-10 l/min |
| " " | hydrogen | 0-0.5 l/min |
| " " | methane/acetylene | 0-1 l/min |
| pressure vacuum system | | 0.1-10 mbar |
| substrate bias voltage | | 0-200 V |

The auxiliary discharge. As already mentioned section the sample support is electrically isolated from the vacuum system. It is connected to a power supply with a series resistance to be able to create an auxiliary discharge which negatively biases the sample support. As the major part of the discharge voltage drop takes place over the cathode fall region, the energy of the ions impinging on the substrate surface can be tuned from 0 Volt to 200 Volt. The power that is dissipated in the discharge (about 20 Watts) is small compared to the energy present in the plasma beam, so it is reasonable to assume that the gas temperature and dissociation degree of the plasma beam are hardly influenced by this auxiliary discharge.

## The optical systems and diagnostics

Introduction. For observation of the dense cascaded arc plasma itself an optical fiber is connected directly to a cascaded plate in front of a small quartz window mounted in the plate. The other end of the fiber is put directly in front of the entrance slit of a Jarrell-Ash 0.5 m. monochromator. This construction allows for the measurement of the axial dependences of the electron density and electron temperature. The electron density is determined using the Stark broadening of the Hβ-Balmer line (486.1 nm), the electron temperature by comparing the emissivity of the continuum radiation and of the line radiation of an argon ion line (480.6 nm).

A second optical system has been implemented which allows for the execution of various spectroscopic techniques to measure several parameters of the expanding plasma beam as a function of the position in the plasma. The optical system comprises a 0.5 m monochromator and in the case of high resolution spectroscopy, a pressure scanned Fabry-Pérot interferometer (see Fig. 4).

The electron density is determined using the Stark broadening of the Hβ-Balmer line (486.1 nm). The gas velocity can be deduced from the Doppler shift of the 420.0 argon neutral line, the gas temperature from the width of the Gaussian component of that same line.

In-situ He-Ne laser ellipsometry has been used to determine the deposition rate and the optical film properties at a wavelength of 632.8 nm. A spectroscopic ellipsometer was applied to determine the optical film properties over a wide wavelength area (200-700 nm). It is beyond the scope of this contribution to discuss the ellipsometers in detail. Therefore we will be concise about this matter; for a more extended presentation see (ref. 30).

In the following subsections we will briefly discuss the various physical principles of the used diagnostics, for more details see e.g. (refs. 31, 32, 33).

Broadening and shift of spectral lines. The wavelength-dependent intensity profile of a spectral line emitted in the plasma is determined by several physical effects. Each effect can result in a shift of the line position and in a broadening of the profile, with either a Lorentz- or a Gauss-like contribution. If several broadening effects occur simultaneously the

line profiles will be convoluted. The convolution of two Gauss profiles is also a Gauss profile, and the convolution of two Lorentz profiles is again a Lorentz profile. In the case of Gauss profiles the widths have to be added quadratically, in the case of Lorentz profiles linearly. When a Gauss profile is convoluted with a Lorentz profile a Voigt profile results. Two Voigt profiles convolute to again a Voigt profile.

The spectral lines emitted by the plasma show Doppler broadening. The thermal movements of the radiating atoms cause a Doppler shift in the observed frequencies. If the velocity distribution is taken Maxwellian with a temperature $T$, then the line profile has a Gaussian shape with a full width at half maximum (FWHM) $\gamma$ (in meters) according to

$$\gamma = \lambda_0 \sqrt{(8 \, ln2 \, k_B T/m)} \ . \tag{4}$$

Here $\lambda_0$ represents the centre wavelength, $k_B$ the Boltzmann constant and $m$ denotes the atomic mass.

If all the atoms have an average velocity component $v$ in the direction with an angle $\vartheta$ with respect to the observer, the wavelength of the spectral line appears to be shifted over a range $\Delta\lambda$, with

$$\Delta\lambda = - \lambda_0 \, v \, cos \, \vartheta/c, \tag{5}$$

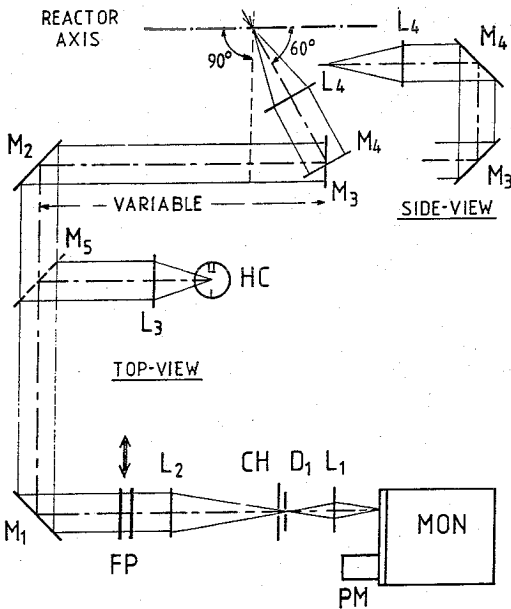where $c$ denotes the velocity of light.



Fig. 4. The optical system. Lenses: $L_1 - L_4$,
Mirrors: $M_1 - M_5$, Diafragma $D_1$,
Monochromator MON, Photomultyplier PM,
Fabry–Perot interferometer FP, Chopper CH,
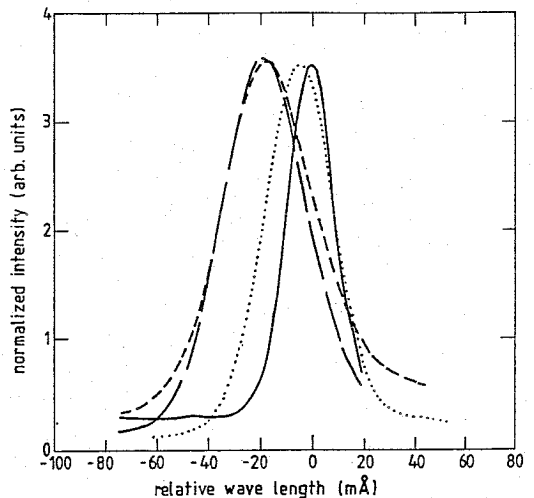Low pressure reference source HC.



Fig. 5. Shift of the argon neutral line 420.0 nm, measured at several axial positions, to the reference line.
———— the reference line,
– – – spectral line at $z$ = 30 mm,
—— —— spectral line at $z$ = 20 mm,
. . . . spectral line at $z$ = 60 mm.

With the monochromator and the pressure scanned Fabry–Pérot interferometer the width of a spectral line profile radiated from the plasma at a certain position can be measured. This measured profile is a convolution of the (mainly Doppler broadened) profile radiating from the plasma and the apparatus profile which is determined by the dispersive and optical properties of the entire optical system. This apparatus profile is analyzed using the same spectral line as it is emitted by a low pressure reference source. The width of this used reference line (argon neutral 420.0 nm) is small (about 0.12 pm) compared to the apparatus profile (about 0.40 pm). Analyzing the apparatus profile yields Lorentz- and Gauss components.

Deconvolution of the measured profile and the known apparatus profile yields the real Gaussian component of the spectral line. With eq. (4) the gas temperature can then be calculated. With the combination of the pressure scanned Fabry–Pérot interferometer, the monochromator and an unshifted spectral line as reference (see Fig. 4) the wavelength shift due to the axial plasma velocity $v$ as observed at the known angle $\vartheta$ can be determined. See Fig. 5 for an example of shifted and unshifted profiles. With eq. (5) the velocity $v$ can be calculated.

The Stark effect is caused by interaction of charged particles and the radiating atom and usually results in a Lorentzian line broadening profile (with the prominent exception of hydrogen atoms). The width is proportional to the electron density. Griem has accumulated the Stark parameters for a large number of atomic transitions (ref. 34]. For the 420.0 nm argon line that is used in the experiments the Stark width is about 0.06 pm, which is negligable compared to the Doppler broadening of about 2 pm.

In the case of hydrogen also ion broadening has to be taken into account. Griem calculated the total width of the hydrogen lines as a function of electron density $n_e$. The result is given by

$$n_e = C \, \Delta\lambda^{3/2} \, , \tag{6}$$

where C is a constant that only slightly depends on the electron temperature and $\Delta\lambda$ is the full width at half maximum (FWHM) of the line. For the $H\beta$-line ($\lambda = 486.1$ nm), for $T_e = 1$ eV, C values $1.2 \cdot 10^{22}$ $m^{-3} nm^{-3/2}$. With the measurement of the width of this hydrogen spectral line (about 50 pm) and the known temperature, the electron density can be determined with eq. (6). The natural line width and the widths caused by other broadening mechanisms, like resonance broadening, van der Waals broadening, etc, are negligibly small.

Line to continuum ratio. The emissivities of line- and continuum radiation, $\epsilon_l$ and $\epsilon_c$ respectively, can be written as

$$\epsilon_l(T_e) = n_p \, A_{pq} \, (h\upsilon/4\pi) \, P_l \quad \text{and} \tag{7}$$

$$\epsilon_c(T_e) = C_1 \, \frac{n_e n_1}{\lambda^2 \sqrt{T_e}} \, (G_1(\lambda,T_e) + (1-exp(-h\upsilon/kT_e))\xi_1). \tag{8}$$

Here

$n_p$ – density of excited level,

$A_{pq}$ – transition probability for level $p$ to level $q$,

$P_l$ – normalized line profile,

$C_1$ – constant ( $1.63 \; 10^{-43}$ $Wm^4 K^{1/2} sr^{-1}$),

$G_1$ – Gaunt factor ($\approx 1.2 \; exp(-h\upsilon/kT_e)$ at $\lambda = 420.0$ nm),

$\xi_1$ – Biberman factor ($\approx 1.55$ at $\lambda = 420.0$ nm),

$n_1$ – ion density (only singly charged ions have been taken into account),

$n_e$ – electron density,

$T_e$ – electron temperature.

Assuming that the plasma is in partial local thermal equilibrium (PLTE) and taking into account the convolution of both emissivities with the apparatus profile, the line to continuum intensity ratio in the top of the line profile can be calculated as a function of the electron temperature.

Implementation of ellipsometry. Ellipsometry is a technique that uses the difference in reflection ratio that occurs when monochromatic electromagnetic waves, polarized parallel respectively perpendicular to the plane of incidence, are reflected at a flat surface. Because of the internal reference of the technique it is very accurate and relatively insensitive to optical imperfections. Essentially two different systems have been used.

The first one is a low-cost monochromatic ellipsometer based on a He-Ne laser that can be used in-situ. The configuration of the rotating analyzer He-Ne ellipsometer is of the standard Polarizer Sample Analyzer (PSA) type (ref. 35). It is employed to monitor the plasma deposition process as far as growth rate of the film and its refractive index (at $\lambda=632.8$ nm) are concerned. To make sure that the fluctuations of the output power of the laser cannot cause any important inaccuracies an intensity- and frequency stabilized He-Ne laser has been used as a light source (ref. 36).

The second one is a spectroscopic ellipsometer which is used to determine the optical parameters of the produced films over a wide wavelength range. This one has not been used in-situ. This spectroscopic ellipsometer also has the PSA configuration. A cascaded arc in argon is used as a light source and the arc design is similar to the one as employed for the deposition reactor itself. The diameter of the arc channel is in this case 2 mm, the arc current is 25 amps., and the argon pressure is 1 atm. Under these conditions the plasma will be close to LTE at a temperature of about 11000 Kelvin. Especially in the UV-region the spectral emittance is rather high.

<u>Data aquisition</u>. All the spectroscopic signals as intensities and the Fabry-Pérot pressures are sampled by a 12 Bit ADC connected to a M68000 micro-computer. This computer also performs the deconvolution calculations and the rather complicated processing of the ellipsometric results. This microcomputer is connected to a LSI-11/23 host-computer with a background memory of 0.5 Gbyte.

## RESULTS

The electron density, the electron temperature and the gas pressure inside the arc channel of the cascaded arc have been determined as a function of axial position for a number of discharge conditions. As an example Fig. 6 presents the curves for two conditions. A general feature in all such measurements is that both the electron temperature and the electron density firstly rise as a function of the distance from the cathode. Then a maximum will be reached after which the temperature and electron density decrease. This is not very surprising because when working at large (buffer) gas flows, as is done here, it simply takes time for the cold gas to get heated, dissociated and ionized. Note the difference in magnitude between the applied argon/hydrogen gas flow and the admixed $CH_4$ or $C_2H_2$ flow. PLTE (partial local thermodynamical equilibrium) calculations yield that the plasma is approaching equilibrium when flowing from cathodes to anode.

Supersonic behaviour clearly shows from the velocity of the neutral atoms in the expanding plasma beam (see Fig. 7 for the centre of the beam). It increases from about 1700 m/s in the nozzle to 3000 m/s at the beginning of the Mach disk. Then it decreases to an equilibrium
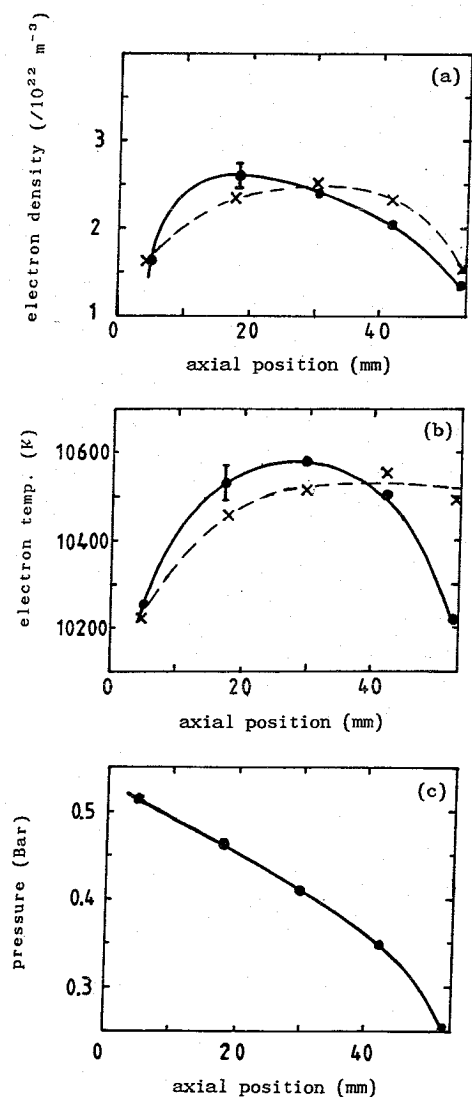


Fig. 6. The electron density (a), the electron temperature (b) and the gas pressure (c) in the cascaded arc channel as a function of axial position.

Plasma conditions
$P_{vac} = 1$ mbar
$I_{arc} = 50$ A

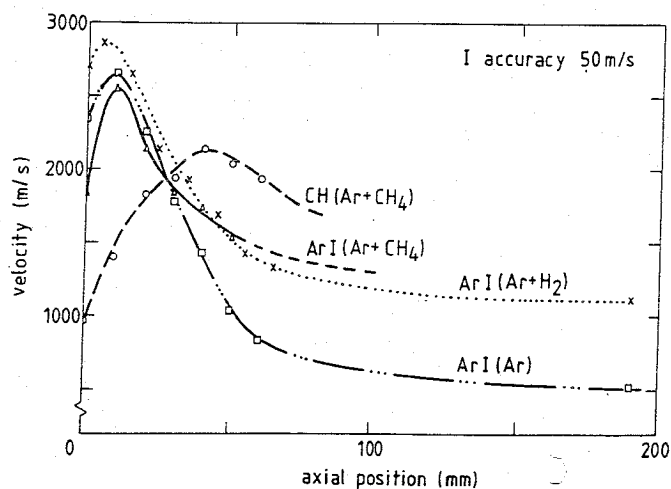| | flow (cc/s) | |
| | drawn line | broken line |
|-----|-----|-----|
| Ar | 100 | 100 |
| $CH_4$ | 0 | 1.0 |
| $H_2$ | 0.30 | 0.30 |



Fig. 7. The gas velocity in the plasma beam as a function of axial position.

value which only depends on the plasma composition. In Fig. 8 a three-dimensional plot of the velocity profile of a pure argon plasma in the expanding beam is given. Notice the beam shape of the expanding plasma even at large distances from the nozzle. The background pressure has no influence on the equilibrium value. The electron density in the plasma beam has been determined as a function of the position in the plasma. Figure 9 presents some typical results of the radial profile of the electron density at several axial positions.

The plasma is operated in a standard condition: $I = 50$ A, argon flux $= 5 \cdot 10^{21}$ s$^{-1}$, carbon flux $= 5 \cdot 10^{19}$ s$^{-1}$ and the background pressure $= 1$ mbar. In each of the Figures 10–16 one of these parameters has been varied without affecting the others.

The deposition rate has been determined as a function of the flux of supplied carbon atoms (Fig. 10). It appears to be perfectly linear and independent of the composition of the admixed gas. The deposition rate as a function of the argon flux is presented in Fig. 11 which shows a maximum at an argon flux of roughly $20.10^{21}$ s$^{-1}$; as a function of the background pressure in Fig. 12 and as a function of arc current in Fig. 13.
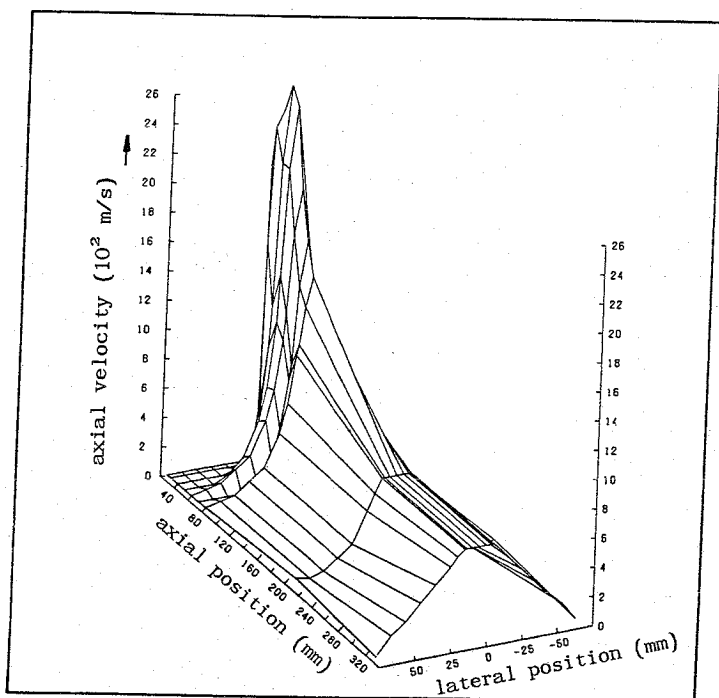


Fig. 8. Three dimensional plot of the axial velocity profile of argon neutral in a pure argon gas.
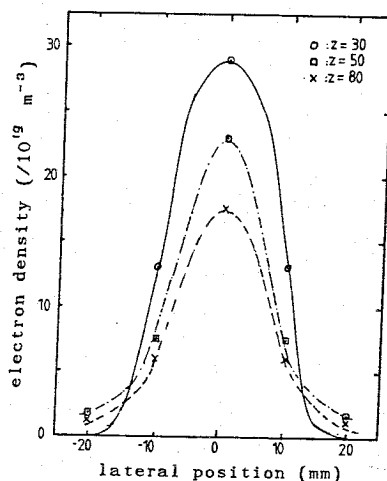


Fig. 9. Lateral profiles of the electron density in the plasma beam at axial positions z = 30, 50 and 80 mm.
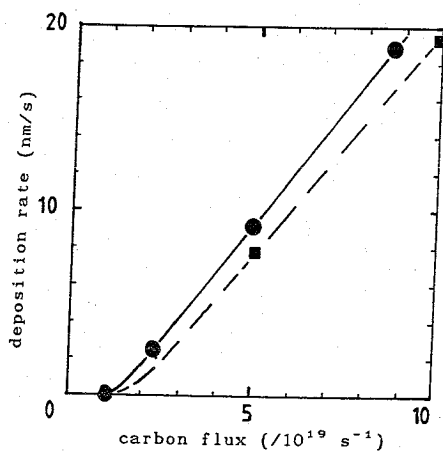


Fig. 10. The deposition rate as a function of the flux of carbon atoms. Dots: methane, squares: acetylene.
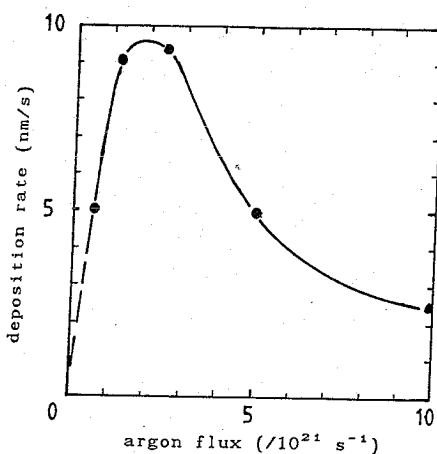


Fig. 11. The deposition rate as a function of the argon flux.

When the discharge conditions change however, not only the deposition rate is influenced but also the film quality. As an illustration the Figs. 14 to 16 depict the refractive index of the produced films as a function of carbon flux, argon flux and arc current respectively. Usually the refractive index is strongly linked with the hydrogen content and the hardness (ref. 37).
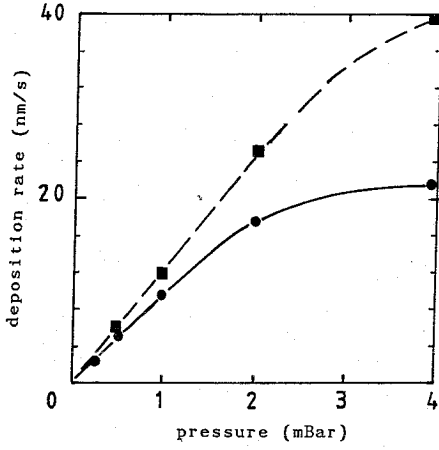


Fig. 12. The deposition rate as a function of background pressure. Dots: methane, squares: acetylene.
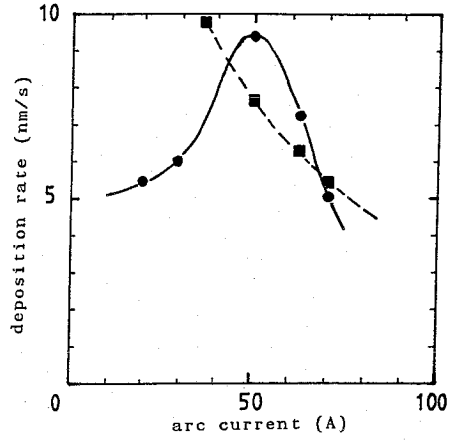


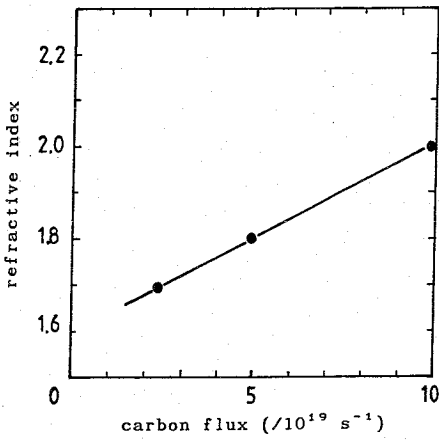Fig. 13. The deposition rate as a function of arc current. Dots: methane, squares: acetylene.



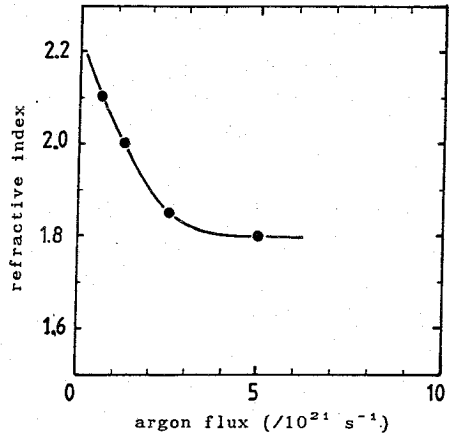Fig. 14. The refractive index of the deposited film as a function of the carbon flux.



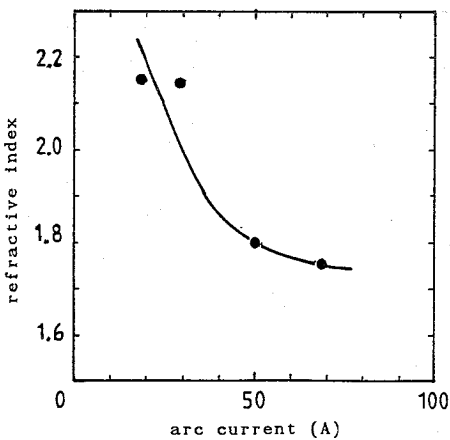Fig. 15. The refractive index of the film as a function of the argon flux.



Fig. 16. The refractive index of the film as a function of the arc current.

## CONCLUDING REMARKS

From Fig. 6 one can conclude that it takes about 15 mm for the cold atoms to get heated, dissociated and partially ionized in the arc channel. Because the gas velocity in the channel is about 1500 m/s the heating time of the particles is about 10 μs. Therefore, if a reactive gas is injected 15 mm before substantial expansion of the plasma into the vacuum chamber takes place, on can assume that it will be completely dissociated. Probably a large fraction of it will be ionized when the fragments have a lower ionization potential than the arc feeding gas (in this case argon).
A further indication that the gas is completely dissociated is given in Fig. 10. It hardly makes any difference whether methane or acetylene is used: as far as the deposition rate is concerned only the number of supplied carbon atoms matters. Apparently it is of no importance that methane and acetylene have distinctly different C:H ratios, viz. 1:4 and 1:1 respectively.

Figure 11 clearly indicates that there is an optimum deposition rate of about 10 nm/s at an argon flux of about $2 \cdot 10^{21}$ s$^{-1}$. If the flux is smaller (and also the arc pressure) then the electron density in the arc is smaller. In that case the reactant will not be dissociated completely and a lower deposition rate results. If the argon flux is larger than the optimum value the energy flux impinging on the surface becomes too large, favouring evaporation and etching processes (ref. 38); the deposition rate will decrease. This phenomenon also occurs if the arc current is chosen too high (Fig. 13). Rising the background pressure has a proportional effect on the deposition rate as long as it stays below 2 mbar (see Fig. 12). As the diameter of the plasma beam is directly linked to the background pressure via the concept of ambipolar diffusion the deposition rate depends linearly on the pressure. Above a threshold value of about 2 mbar the phenomenon discussed before occurs (see the deviation from the linear curve).

One will notice that the deposition rates mentioned above are very high compared to the usual values. By increasing carbon flux, argon flux and arc current at the same time we have attained deposition rates up to 200 nm/s. These values are considerably (a factor 100) higher than the values found in the literature (see e.g. refs. 2 to 18). In our opinion this is the result of overcoming the limitations mentioned in the introduction by geometrically separating the plasma production region and the plasma treatment region. Table 2 illustrates the difference with respect to some fundamental parameters between conventional processes and this deposition process.

TABLE 2. *Comparison of some fundamental parameters.*

| Phase | Parameter | Glow discharge | This work |
|---|---|---|---|
| 1 | material density | $10^{21}$ m$^{-3}$ | $10^{22}$ m$^{-3}$ |
| 1 | electron density | $10^{17}$ m$^{-3}$ | $10^{22}$ m$^{-3}$ |
| 1 | electron temperature | 3 eV | 1 eV |
| 1 | gas temperature | 400 K | 10000 K |
| 1 | power consumption | ≈ 100 W | ≈ 10 kW |
| 2 | transport velocity | 100 m/s | 2000 m/s |
| 2 | flux ratio | ≈ 0.1 | ≈ 1 |
| 2 | electron density | $10^{17}$ m$^{-3}$ | $10^{19}$-$10^{20}$ m$^{-3}$ |
| 2 | gas temperature | 400 K | 5000-1500 K |
| 3 | deposition rate | ≤ 2 nm/s | ≤ 200 nm/s |
| 3 | potential energy (all particles averaged) | < .1 eV | > 1 eV |

Summarizing one can mention that it has been worthwile to separate the plasma production region from the treatment region as is done in the experiment descibed; it gives more freedom to optimize the deposition process. It is advantageous to use a thermal plasma in the plasma production part.
The thermal plasma of a cascaded arc is very suitable as a source of reactive particles. At relatively high current densities (40-70 amps through a 4 mm channel) and at normal working pressures (p > 0.5 bar) there are only minor deviations from local thermodynamical equilibrium (LTE) at a temperature about 11000 K. In this plasma each injected molecular particle

is dissociated immediately and in many cases ionized quickly. At lower currents (5-25 A) the deviations from LTE become substantial and in low pressure arcs (p < 0.2 bar) the gas temperature can be significantly lower than the electron temperature. If the reactive gas is not injected directly into the arc plasma but at the location of the supersonic expansion or even further downstream, the plasma beam is strongly quenched and molecular species can survive. By carefully selecting arc pressure, gas flow, arc current and injection location the composition of the plasma beam on one hand and its potential and kinetic energy content on the other hand can be influenced independently. The kinetic energy of the ions impinging on the surface can be increased by applying an auxiliary discharge. In this way this plasma can provide the optimum surface environment and particle fluxes for the deposition of a wide range of materials on almost any substrate. The experiment has been carried out with hydrocarbons to produce amorphous hydrogenated carbon films (a:C-H) but the setup is not limited to this material. By chosing another starting material (e.g. $SiH_4$, $TiCl_4$ and $N_2$, etc) semiconductor and/or metallic alloy films can be produced.

## Acknowledgement

## REFERENCES

1. H. Borning, Plasma News Report, Carlsbad, CA, USA, sept. (1986).
2. T. Matsushita, K. Komori, M. Konagai and K. Takahashi, Appl. Phys. Lett. 44(1984)1092.
3. T.J. Donahue and R. Reif, J. Appl. Phys. 57(1985)2757.
4. P.E. Vanier, F.J. Kampas, R.R. Corderman and G. Rajeswaran, J. Appl. Phys. 56(1984)1812.
5. J. Wong, T.M. Lu and S. Mehta, J. Vac. Sci. Techn. B(1985)453.
6. K. Ebihara and S. Maeda, J. Appl. Phys. 57(1985)2482.
7. M. Sokolowski et al, Thin Solid Films 80(1981)249.
8. K. Umeda, Y. Kawashimo, M. Nakasone, S. Harada and A. Tasaki, Jap. J. Appl. Phys. 23(1984)1576.
9. M. Shindo, S. Sato, I. Myokan, S. Mano and T. Shibata, Jap. J. Appl. Phys. 23(1984)273.
10. Y. Toyoshima, K. Kumata, U. Itoh, K. Arai, A. Matsuda, N. Washida, G. Inoue and K. Katsuumi, Appl. Phys. Lett. 46(1985)584.
11. T. Watanabe, K. Azuma, M. Nakatani, K. Suzuki, T. Sonobe and T. Shimada, Jap. J. Appl. Phys. 25(1986)1805.
12. S. Matsumura, K. Sakurai, A.A. Berezin, R.M. Hobson, S. Teii and J-S. Chang, Can. J. Phys. 63(1985)826.
13. A. Lunk and M. Schmidt, Proc. ESCAMPIG VIII, Greifswald, DDR, p. 37, (1986).
14. C.B. Zarowin, N. Venkataramanan and R.R. Poole, Appl. Phys. Lett. 48(1986)759.
15. P. Rutérana, P. Friedel, J. Schneider and J.P. Chevalier, Appl. Phys. Lett. 49(1986)672.
16. J. Perrin, Ph. D. Thesis, Université Paris VII (1983).
17. J. Kieser and M. Neusch, Thin Solid Films 118(1984)203.
18. H. Yamada and Y. Torii, Appl. Phys. Lett. 50(1987)386.
19. R.J. Rosado, An investigation of non-equilibrium effects in thermal argon plasmas, Ph. D. thesis, Eindhoven University of Technology, Eindhoven, The Netherlands, (1981).
20. C.J. Timmermans, R.J. Rosado, and D.C. Schram, Z. Naturf. 40a(1985)810.
21. K. Akashi, Pure & Appl. Chem., 57-9 (1985)1197.
22. H. Mäcker, Z. Naturforsch. 11a(1956)457.
23. S. Vacquie, A. Gleizes and H. Kafrouni, J. Phys. D: Phys. 18(1985)2193.
24. A. Gleizes, I. Sakalis, M. Razafinimanana and S. Vacquie, J. Appl. Phys. 61(1987)510.
25. H.Kafrouni, J.M. Bagneaux, A. Gleizes and S. Vacquie J. Quant. Spectrosc. Radiat. Transfer 21(1979)457.
26. T.L. Eddy, C.J. Cremers and H.S. Hsia, J. Quant. Spectrosc. Radiative Transfer 17(1975)287.

27. U.H. Bauder, Appl. Phys. 9(1976)105.
28. C.J. Timmermans, An investigation of pulsed high density plasmas, Ph. D. thesis, Eindhoven University of Technology, Eindhoven, The Netherlands (1984).
29. J.C.M. de Haas, Ph. D. thesis, Eindhoven University of Technology, "Non-equilibrium in flowing atmospheric plasmas" (1986).
30. G.M.W. Kroesen and D.C. Schram, Proc. ICPIG XVIII, Swansea, U.K. (1987).
31  H.R. Griem, Plasma Spectroscopy, MacGraw Hill, New York (1964).
32. I.I. Sobelman, Introduction to the theory of atomic spectra, Pergamon Press, Oxford (1972).
33. G. Traving, Plasma Diagnostics, Ed. by W. Lochte-Holtgreven, North-Holland Publ. Comp., Amsterdam, The Netherlands (1968).
34. H.R. Griem, Plasma Spectroscopy, MacGraw Hill, New York (1964).
35. R.M.A. Azzam, N.M. Bashava, Ellipsometry and Polarized light, North-Holland Publish. Comp., Amsterdam (1977).
36. G.M.W. Kroesen, Private communication, intern report, University of Technology, Eindhoven, The Netherlands, Department of Physics, VDF/NT-87-06 (1981).
37. G.M.W. Kroesen and S.S. Klein, to be published.
38. K. Enke, Proc. E-MRS conference Strasbourg, session C, to be published (1987).